

# Channel modeling and MIMO capacity for outdoor millimeter wave links<sup>1</sup>

Hong Zhang, Sriram Venkateswaran and Upamanyu Madhow  
 Department of Electrical and Computer Engineering  
 University of California, Santa Barbara  
 Email: {hongzhang, sriram, madhow}@ece.ucsb.edu

**Abstract**—Recent work has shown that mesh networks based on short-range outdoor millimeter (mm) wave links in the unlicensed 60 GHz band are a promising approach to providing an easily deployable broadband infrastructure. In this paper, we investigate the robustness of such links, focusing in particular on the effect of multipath fading resulting from reflections from the ground and building walls for a lamppost deployment of mm wave nodes. Our ray tracing based model shows that, while only a small number of paths are significant for the highly directional links considered, they can cause significant fluctuations in the received signal strength. Our simulations show that 10-20 dB fades below the benchmark of free space propagation can occur quite easily (e.g., 5-15% of the time, averaging across typical deployment scenarios), and that the received power is extremely sensitive to small variations in geometry (e.g., altering the position of the antenna by 1 cm can reduce the received power as much as 46.7 dB). We also demonstrate, however, that extremely robust performance can be obtained by employing multiple antennas at appropriately chosen separations, using standard space-time communications strategies such as transmit precoding (when the transmitter knows the channel) and space-time coding (when the transmitter does not know the channel).

## I. INTRODUCTION

The increasing demand for high-definition multimedia and high speed computer communications has led to the need for a new generation of wireless networks that support higher data rates. The 60 GHz band is considered to be a promising candidate for building such high speed, short range wireless networks for a number of reasons: it offers large swathes of unused bandwidth (57-64 GHz) and has a high spatial frequency reuse because of significant attenuation due to oxygen absorption [1]. Crucially, recent advances in RFIC design have made millimeter wave (mm-wave) transceivers using *inexpensive* silicon processes feasible [2][3]. While there is intense industry interest in multiGigabit 60 GHz indoor networks [4], recent work [5] shows that *outdoor* mesh networks based on short-range (100s of meters) 60 GHz links are a promising approach to providing a quickly deployable multiGigabit wireless backhaul (e.g. for picocellular networks or for “last-hop” links in a neighborhood). In this paper, we investigate space-time channel models for such links, which turn out to be very different from those at lower carrier frequencies. We also discuss the consequences for transceiver design.

The differences between mm-wave and WiFi networks at 2.4 and 5 GHz stem from the order of magnitude difference in wavelength  $\lambda$  of the carrier used for transmission. Since

free space propagation loss scales as  $\lambda^2$ , the propagation loss in mm-wave networks is 28 dB higher than the loss in WiFi networks (at 2.4 GHz). On the other hand, the antenna directivity scales as  $\lambda^{-2}$  for an antenna with a given aperture (corresponding to nodes with a fixed form factor). Therefore, using directional antennas at both the transmitter and the receiver leads to a net power scaling of  $\lambda^{-2}$ , which translates to an advantage of 28 dB for 60 GHz versus 2.4 GHz. Since it is difficult to produce high transmit powers using low-cost silicon implementations, the use of directional transmission and reception is imperative at 60 GHz. Fortunately, the smaller wavelength also makes it possible to synthesize low-cost antenna arrays (e.g., implemented as patterns of metal on circuit board), which can then be electronically steered to provide adaptive yet highly directional links permitting a flexible deployment. From the point of view of channel modeling, the consequence of directionality is that the channel between the transmitter and receiver is dominated by a few paths which fall within the transmit and receive antenna beamwidths. This is fundamentally different from the much richer scattering environment for omnidirectional links at lower carrier frequencies.

**Contributions:** We employ ray tracing technique to characterize the multipath channel associated with highly directional 60 GHz links. While only a few rays fall within the antenna beamwidths, the strength of these rays is of the same order as that of the Line of Sight (LOS) path, so that constructive and destructive interference between the rays causes severe fades. In particular, because of the small wavelength, small changes in geometry of the environment are shown to result in large fluctuations in received signal strength. This implies, for example, that a link with a single  $\frac{\lambda}{2}$ -spaced antenna array at each end is not robust. However, the small wavelength also implies that spatial diversity is easy to achieve; two directional antennas (or steerable antenna arrays) which are judiciously placed at a moderate distance apart result in a robust  $2 \times 2$  MIMO link to which standard space-time communication techniques apply. In particular, we employ Shannon-theoretic computations for both transmit precoding and space-time coding schemes to show that a large stable throughput can be achieved.

**Related Work:** There have been a number of studies of statistical channel models as well as measurement campaigns in the 60 GHz band in *indoor* environments [6][7][8][9]. The significant difference between these indoor studies and the outdoor environment we consider is the impact of larger transmission range and stronger reflected rays. It has been shown in Reference [10] that only the Line of Sight (LOS)

<sup>1</sup>This research was supported in part by the National Science Foundation under grants CNS-0520335, ECS-0636621 and CNS-0832154.

ray needs to be considered in the indoor environment when the transmission range is less than 10 meters. References [11] and [12] study an outdoor channel model in a city street environment; however, they investigate the channel response in the 2 GHz band with *omnidirectional* antennas. As we show in this work, the directional antennas needed for 60 GHz nodes lead to significantly different channel models when compared to lower frequency, omnidirectional networks. In terms of 60 GHz *networks*, reference [5] shows that oxygen absorption and the use of highly directional links allows a high degree of spatial reuse. It also shows that directionality leads to a drastically different design paradigm for Medium Access Control (MAC) protocols, with the focus shifting away from interference management (since interference is greatly reduced due to directionality) to transmit-receive coordination (because the “deafness” caused by directionality makes carrier sense based protocols infeasible). While [5] considered idealized LOS link models, more detailed network design and performance studies require a fundamental understanding of the channel model for such links, which is the objective of the present study.

## II. CHANNEL MODEL AND PROPERTIES

To understand the outdoor channel characterization, the environment geometry of the outdoor channel considered throughout the paper is described, following which we describe the calculation of reflection coefficients and a sample link budget. We then show that while there are only a small number of dominantly reflected rays, the received signal strength fluctuates significantly even with small scale variations in the environment.

### A. Environment Geometry

We model an outdoor mm-wave network with the nodes deployed on lamp-posts, which are typically lower than the rooftops. The street on which the lamp-posts are located is assumed to be straight, with buildings *throughout* the sides of the street. These buildings cause reflected rays to be received in addition to the direct path: the reflected rays could add either constructively or destructively, leading to the well-known fading effects. Note that the assumption of buildings *throughout* the street leads to a worst-case scenario: in practice, the absence of tall buildings at street intersections might cause fewer reflected rays which would, in turn, lead to diminished fading effects. The canonical environment geometry we consider is shown in Fig. 1: (a) the transmitter and the receiver are placed at the top of the lamp posts on the same side of the street, (b) the buildings are located  $d_{wall}$  (also called wall distance) meters away from the lamp-posts and (c) the width of the street is denoted by  $l$ . The propagation distance, denoted by  $d_s$ , is typically on the order of 100 m.  $\theta_i$  denotes the incident angle and the complementary angle of  $\theta_i$  is called the direct angle ( $\alpha_i$ ) for convenience. In addition to the reflections from buildings, we also model the reflection from the road, which is not shown in the figure.

### B. Reflection Models

At a vacuum-material interface, the electromagnetic waves undergo a change in gain and phase described by the Fresnel

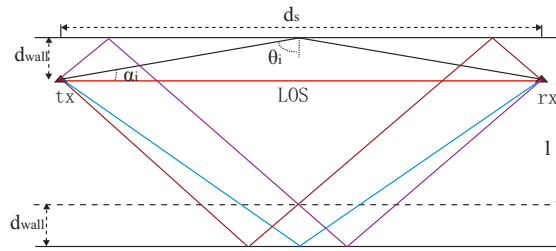


Fig. 1. Top-down view of outdoor propagation geometry illustrating LOS and wall reflected paths up to the second order

reflection coefficients [13]. We now summarize the main results from electromagnetic theory needed for our purpose. We consider electromagnetic waves impinging on a vacuum-material interface that is *smooth and infinite*, with the material having relative dielectric constant  $\epsilon'$ , relative permeability  $\mu'$  and conductivity  $\sigma$ . The *relative complex dielectric constant* for the material, denoted by  $\epsilon_r$ , is given by  $\epsilon_r = \epsilon' - j \frac{\sigma}{2\pi f \epsilon_0}$ , with  $\epsilon_0 = 8.854 \times 10^{-12} \text{ AS/Vm}$ . The perpendicular reflection coefficient  $R_{\perp}$  that relates the reflected and incident electric fields when the polarization perpendicular to the plane of incidence, is given by

$$R_{\perp}(\theta_i) = \frac{E_{\perp,r}(\theta, i)}{E_{\perp,i}(\theta, i)} = \frac{\cos \theta_i - \sqrt{\mu' \epsilon_r - \sin^2 \theta_i}}{\cos \theta_i + \sqrt{\mu' \epsilon_r - \sin^2 \theta_i}} \quad (1)$$

where  $\theta_i$  denotes the angle of incidence. Analogously, when the polarization is parallel to the plane of incidence, the parallel reflection coefficient  $R_{\parallel}$  is given by

$$R_{\parallel}(\theta_i) = \frac{E_{\parallel,r}(\theta, i)}{E_{\parallel,i}(\theta, i)} = \frac{\mu' \epsilon_r \cos \theta_i - \sqrt{\mu' \epsilon_r - \sin^2 \theta_i}}{\mu' \epsilon_r \cos \theta_i + \sqrt{\mu' \epsilon_r - \sin^2 \theta_i}} \quad (2)$$

If we use vertical polarization, the wall and ground reflection coefficients are equal to  $R_{\perp}$  and  $R_{\parallel}$  respectively.

The Fresnel reflection coefficients are strictly valid only with infinite and smooth surfaces. However, a surface can be approximated as electromagnetically “smooth” if its irregularities are small. The *Rayleigh criterion* provides a thumb rule to capture the extent of irregularities: a surface may be approximated to be smooth if  $h < \frac{\lambda}{8 \cos \theta_i}$ , where  $h$  denotes the maximum irregular height of the material surface and  $\theta_i$  represents the angle of incidence. For rough surfaces, a multiplicative scattering loss factor  $\rho_s = \exp \left[ -\frac{1}{2} \left( \frac{4\pi \sigma_h \cos \theta_i}{\lambda} \right)^2 \right]$  [13] is used to account for the reduced energy in the reflected ray, where  $\sigma_h$  denotes the standard deviation of the surface height. However, what we consider here is the simple but worst case by assuming all the surfaces are smooth enough, which leads to the highest reflected power and hence larger fades.

### C. Link Budget and Antenna Design

We now lay out the link budget of an example system that we consider throughout the paper. Consider a 2 Gbps QPSK link, over a distance of 200 m, operating with a bandwidth of 1.5 GHz. For uncoded Bit Error Rates (BERs) lower than  $10^{-9}$ , the required signal-to-noise ratio (SNR) is 14 dB. Assuming that the oxygen absorption loss is 16 dB/km, and antenna directivities at each end of 20 dBi, we find that the required transmit power is 24 dBm with a link margin of 10

dB and a receiver noise figure of 5 dB. We have not budgeted for rain, which can lead to significantly higher attenuation and hence call for smaller range, higher transmit power, or even higher antenna directivities. This is because our goal is to highlight the need for high directivities even under ideal conditions, and to investigate fading as a function of range up to what we currently think is the maximum range feasible with low-cost silicon implementations.

**Antenna Design:** A directivity of 20 dBi can be realized, for example, using an antenna (or an antenna array) with  $30^\circ$  vertical beamwidth and  $10^\circ$  horizontal beamwidth. A possible low-cost implementation is to employ a 4-element linear array of endfire antenna elements with  $40^\circ$  horizontal beamwidth and half-wavelength spacing. The antenna radiation patterns for one such element, which could be realized as a pattern of metal on circuit board [14], are shown in Figures 2(a) and 2(b). For concreteness, we use these patterns in our channel model simulations.

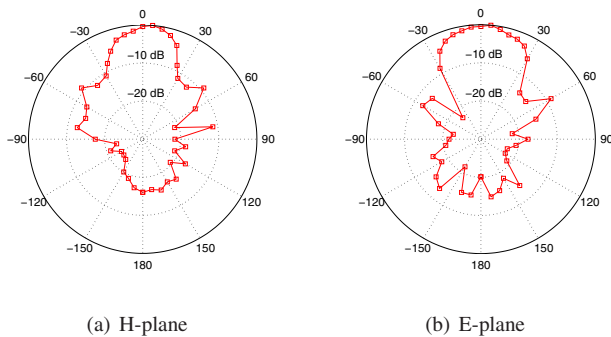


Fig. 2. Endfire antenna power pattern with a directivity of 14 dBi

#### D. Six-ray Channel Model

Owing to the narrow horizontal beamwidth of the receive antenna, only rays with small direct angles (see Fig. 1) make a significant contribution towards the received signal. Defining the *order* of a reflected ray to be the number of reflections the ray undergoes before reception, we see from Fig. 1 that higher order rays have larger direct angles which fall outside the beamwidth. For the geometries and directivities that we consider, we find that it suffices to consider only reflected rays up to the second order to account for the signal contribution at the receiver from wall reflected paths. For example, consider the following parameters: street width ( $l$ ) of 12 m, wall distance ( $d_{wall}$ ) of 4 m, the lamp post height (antenna height  $h_{ant}$ ) of 5 m, and propagation range ( $d_s$ ) of 200 m. The corresponding 1st and 2nd order direct angles ( $\alpha_i$ ) from both sides of the street are  $2.3^\circ$ ,  $9.1^\circ$  and  $13.5^\circ$ ,  $19.8^\circ$ , respectively. Since the horizontal beamwidth is only  $10^\circ$ , it is clear that considering wall reflections up to the 2nd order is a good approximation.

We therefore consider a six-ray channel model, which accounts for the Line of Sight (LOS) path, the ground reflection ray, and 1st and 2nd order wall reflected rays from buildings on either side of the road. Using the complex baseband representation, the received signal is given by [16]

$$r(t) = \frac{\lambda}{4\pi} \left( \frac{\sqrt{G}u(t)e^{-j2\pi d_s/\lambda}}{d_s} + \sum_{i=1}^5 \frac{R_i \sqrt{G_i} u(t - \tau_i) e^{-j2\pi d_i/\lambda}}{d_i} \right) \quad (3)$$

where (1)  $u(t)$  is the complex baseband transmitted signal, (2)  $\sqrt{G}$  and  $\sqrt{G_i}$  are the *products* of the corresponding transmit and receive antenna field radiation pattern for the LOS component and the reflected components respectively, (3)  $d_s$  is the LOS path length and  $d_i$  is the length of the  $i^{th}$  reflected path, (4)  $R_i$  denotes the *net* reflection coefficient on the  $i^{th}$  path and (5) the delay spread  $\tau_i = (d_i - d_s)/c$  is the difference in propagation delay between the LOS and the reflected rays.

If the bandwidth of the received signal is smaller than the coherence bandwidth (roughly the inverse of the delay spread),  $u(t - \tau_i)$  can be approximated by  $u(t)$ . While this is not quite true for the multiGigabit links of interest (e.g., a delay spread of several nanoseconds leads to a coherence bandwidth smaller than a GHz), we make this approximation in order to focus on channel variations due to spatial geometry. The received signal power is then given by

$$P_r = P_t \left( \frac{\lambda}{4\pi} \right)^2 \left| \frac{\sqrt{G}}{d_s} + \sum_{i=1}^5 \frac{R_i \sqrt{G_i} e^{-j\Delta\phi_i}}{d_i} \right|^2 \quad (4)$$

where  $\Delta\phi_i = 2\pi(d_i - d_s)/\lambda$ . We first analyze the variation of the received power with the same settings as before:  $d_s = 200$  m,  $d_{wall} = 4$  m,  $h_{ant} = 5$  m,  $l = 12$  m. We see from Fig. 3 that the received signal power fluctuates significantly for larger link ranges. In fact, for some link ranges, the received power could be as much as 25 dB lower than the corresponding value in free space (denoted by  $P_{r,fs}$ ) because of the destructive interference caused by the reflected rays.

#### E. Statistical Distribution of the Received Signal Power

In the previous example, we analyzed the variation in received signal power under the assumption of fixed lamp post height and wall distance. However, lamp post heights and wall distances could vary significantly across different network deployments, or even within a given deployment. Furthermore, some variation (on the order of a few centimeters) in the positioning of antennas is inevitable. We would certainly desire the link to be robust to all such variations. We now show that, due to the small wavelength, even small spatial variations can lead to significant fluctuations in the received power. To this end, we introduce a statistical model, in which we compute the distribution of the received power as we vary the wall distance and antenna height, modeling the latter parameters as random variables. In particular, we model the antenna height  $h_{ant}$  as uniformly distributed over the interval [5m,8m], and the wall distance  $d_{wall}$  as uniform over [4m,20m]. The ranges are chosen such that the contributions from the reflected rays are significant over the nominal range  $d_s = 200$ m and nominal street width  $l = 12$ m.

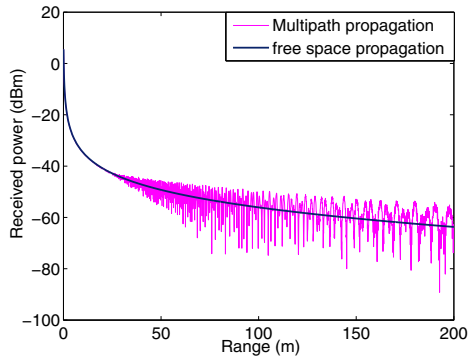


Fig. 3. Received signal power of the SISO channel as a function of the transmission range

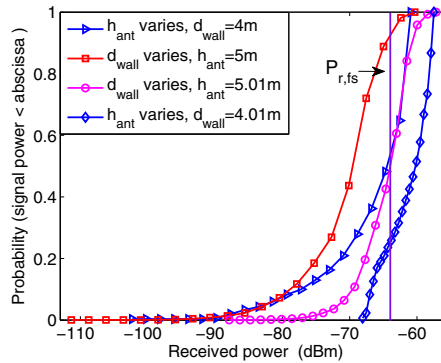


Fig. 4. CDF of received signal power of the SISO channel

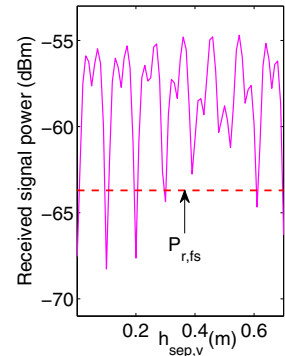


Fig. 5. Received signal of 2x2 MIMO as  $h_{sep,v}$  varies

In Fig. 4, we plot the Cumulative Distribution Function (CDF) of the received power upon varying either the wall distance or the antenna height, keeping the other parameter fixed. The received signal power exhibits significant fades below the free space propagation value  $P_{r,fs}$ : for example, when  $d_{wall}$  varies with the antenna height fixed at 5 m, the reflected paths combine destructively and lead to a lower signal power 93.8% of the time, with 10 dB fades almost 20% of the time and 20 dB fades about 5% of the time. Moreover, the mean signal power can vary by 6 dB when the wall distance or the antenna height changes by as little as 1 cm. However, an even more disturbing observation, not captured in Fig. 4, is the extreme sensitivity of received power to small perturbations in the geometry. For example, when  $d_{wall} = 19.06$  m, the received power for  $h_{ant} = 5.01$  m is  $-64.92$  dBm (a 1 dB fade relative to the free space benchmark of  $-63.7$  dBm), while it is only  $-111.62$  dBm when  $h_{ant}$  is 5 m, corresponding to more than a 48 dB fade!

The preceding results make it clear that some form of spatial diversity is essential in the design of the envisioned 60 GHz outdoor mesh networks. In the next section, we show that appropriately designed  $2 \times 2$  MIMO links do provide such robustness.

### III. MIMO DIVERSITY

We now explore the use of multiple antennas at the transmitter and receiver to utilize spatial diversity and ensure that the links are robust to inevitable environmental variations. We investigate a Multiple Input Multiple Output (MIMO) system with 2 antennas at the transmitter as well as the receiver. Ignoring time dispersion, we have the following model for the spatial channel:

$$\mathbf{y} = \mathbf{H}\mathbf{x} + \mathbf{w} \quad (5)$$

where (1)  $\mathbf{y}$  denotes the  $2 \times 1$  received signal vector, (2)  $\mathbf{H}$  represents the  $2 \times 2$  channel matrix, (3)  $\mathbf{x}$  denotes the  $2 \times 1$  transmitted signal vector and (4)  $\mathbf{w}$  is the  $2 \times 1$  additive white complex Gaussian noise vector with covariance matrix  $\mathbf{C}_w = \begin{bmatrix} N_1 & 0 \\ 0 & N_2 \end{bmatrix}$ . The elements of the channel matrix are obtained by applying ray tracing techniques described in Section II-D to each transmit-receive antenna pair, taking into account the LOS path and ground and wall reflections.

We use Shannon capacity as a compact means of illustrating the performance gains obtainable by going from a SISO to a MIMO link in our context. We note, of course, that hardware constraints at multiGigabit speeds may limit the achievable spectral efficiency to far below these information-theoretic benchmarks. We consider the following standard strategies [15][16][17], reviewed briefly for the sake of completeness.

**Waterfilling:** When the transmitter and receiver have perfect Channel State Information (CSI), the data rate can be maximized by optimally allocating the transmit power to different transmit antennas. The corresponding channel capacity  $C$  is given by  $C = \sum_i (\log_2(1 + \beta_i^2 \frac{P_i}{N_i}))$  [15],  $\beta_i$  is the  $i^{th}$  singular value of  $\mathbf{H}$ ,  $P_i$  and  $N_i$  are the transmit power and noise power at the  $i^{th}$  channel.

**Dominant Eigenmode Transmission:** When link reliability is more important than high data rate, for the same scenario of perfect CSI at both transmitter and receiver, we can transmit information bearing symbols only along the dominant eigenmode of  $\mathbf{H}$  to maximize the SNR at the receiver. The channel capacity is given by  $C = \log_2(1 + \beta_{max}^2 \gamma)$ , where  $\beta_{max}$  is the largest singular value of the channel matrix  $\mathbf{H}$  and  $\gamma$  equals the SNR for the Single Input Single Output (SISO) channel. This channel capacity clearly has an SNR gain of  $\beta_{max}^2$  over the SISO channel [16].

**Alamouti Code:** When the transmitter has no CSI, but the receiver has perfect CSI, the Alamouti scheme [17] maximizes the diversity gain by transmitting repeated symbols through 2 antennas. The capacity is given by  $C = \log_2(1 + \frac{\|\mathbf{H}\|_F^2 \gamma}{2})$ .

**Antenna Separation:** All of the schemes discussed above rely on the channel response between different antenna pairs being roughly independent in order to achieve robust performance. With omnidirectional antennas and a rich scattering environment, the minimum antenna separation required for the paths to observe independent fades can be as small as  $\frac{\lambda}{2}$  [16]. However, with highly directional antennas, the reflected paths that contribute to the received signal lie in a narrow beam around the LOS path, which can lead to significant correlation between the channel responses for different antenna elements. As discussed in detail below, we find that the antenna separation needs to be of the order of  $5\lambda$  for our setting. However, this separation is still relatively small for

the small wavelengths of interest to us.

Both vertical diversity and horizontal diversity are required in order to overcome the fading caused by the ground and wall reflections, respectively. To gain insight, let us first consider only the ground reflected ray and the LOS ray for a  $2 \times 2$  MIMO system with vertically separated antennas spaced by  $d_{sep,v}$ . The received signal power is plotted as a function of the vertical antenna separation when  $d_s = 200$  m and  $h_{ant} = 5$  m. The dependence on the ground surface material is negligible because the reflection coefficient approximately equals -1 regardless of the material when the incident angle is near  $90^\circ$ . Our empirical observation from Fig. 5 is that a vertical antenna separation of  $0.025$  m ( $5\lambda$ ) is a good choice, since this is where the received signal power attains its first peak.

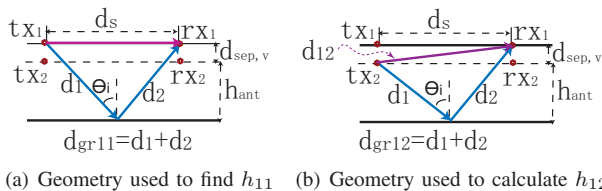


Fig. 6. Front view of propagation geometry with  $2 \times 2$  antennas depicting ground reflections and LOS rays

We next attempt to provide some insight into the preceding empirical observation through ray tracing based calculations. Recall that the sum of the singular values of the channel matrix  $\mathbf{H}$  can be expressed as:  $\sum_i \beta_i^2 = \text{tr}(\mathbf{H}\mathbf{H}^H) = \|\mathbf{H}\|_F^2 = \sum_{i,j=1}^2 |h_{ij}|^2$ . Due to the symmetry in our geometry,  $h_{12} = h_{21}$ . Without loss of generality, we fix the antenna height of  $tx_2$  and  $rx_2$  and vary only the height of  $tx_1$  and  $rx_1$ . Thus,  $h_{22}$  does not depend on the antenna separation. As a consequence, we only need to understand the variations in  $h_{11}$  and  $h_{12}$  with antenna separation. From Fig. 6(a) and Fig. 6(b), the path length of the ground reflected ray in  $h_{12}$  can be expressed as:  $d_{gr12} = d_s / \cos(\arctan(2(h_{ant} + d_{sep,v})/d_s))$ . Assuming that the reflection coefficients are equal to  $-1$  (which corresponds to a phase change of  $\pi$ ), the phase difference between the ground reflected path and the LOS path is  $2\pi(d_{gr12} - d_{12})/\lambda + \pi$ , where  $d_{12} = \sqrt{d_s^2 + d_{sep,v}^2}$ . Similarly, the path length of the ground reflected ray in  $h_{11}$  can be expressed as  $d_{gr11} = 2\sqrt{0.25d_s^2 + (d_{sep,v} + h_{ant})^2}$  and the phase difference is  $2\pi(d_{gr11} - d_s)/\lambda + \pi$ . Using these formulae, we predict the peaks and troughs of  $|h_{11}|$  and  $|h_{12}|$  as the antenna separation varies and list the results in Table I. We find that the predicted trends for the received signal power (low/high/medium) in Table I match the simulated trends in Fig. 5, thereby confirming our insight.

TABLE I

ELEMENTS OF CHANNEL MATRIX VARY WITH ANTENNA SEPARATIONS (B, P AND M DENOTE BOTTOM, PEAK AND MEDIUM POINTS)

	$1\lambda$	$5\lambda$	$10\lambda$	$15\lambda$	$20\lambda$
$h_{11}$	B	P	B	P	B
$h_{12}$	B	M	P	M	B
Total	B	P	M	P	B

In a similar fashion, we find that  $2.5$  cm is also an

appropriate horizontal antenna separation for  $d_s = 200$  m,  $d_{wall} = 4$  m. Hence, the two antennas at each end are placed at the vertices along the vertical face diagonal of a cube with the edge of  $0.025$  m. The later simulations prove that these antenna separations are robust with the variations of the antenna positions and transmit ranges in our scenario.

#### IV. NUMERICAL RESULTS

We now present numerical results that quantify the channel capacity and the received signal power with the three proposed schemes: waterfilling, dominant eigenmode transmission and Alamouti Space-Time Code. We choose the antenna separation to be  $5\lambda = 2.5$  cm as described in Section III. The link budget is described in Section II-C and the reflection coefficients for different materials are found in [18].

**Received Signal Power:** To compare the received signal power in the  $2 \times 2$  MIMO system with the free space propagation case, we define the *Relative Factor*  $\alpha$  as:  $C = \log_2(1 + \alpha SNR_{fs})$ , where  $SNR_{fs}$  denotes the corresponding SNR with free space propagation. Obviously, the MIMO channel can achieve better performance than the free space propagation case if  $\alpha > 1$ . We observe the distribution of the Relative Factor  $\alpha$  upon varying either the antenna height or the wall distance over the same range discussed in Section II-E. The Relative Factor is shown in Fig. 7, where  $\alpha_1$  and  $\alpha_2$  represent the Relative Factors for the corresponding channel with the first or second eigenmode respectively,  $\alpha_{alamouti}$  denotes the Relative Factor using Alamouti scheme. We make the following observations from our simulations:

- 1) We observe from Fig. 7 that the dominant eigenmode transmission scheme using only the largest singular value  $\beta_1$ , which maximizes the received SNR, has the highest Relative Factor ( $\alpha_1$ ) when either the wall distance or the antenna height is varied.
- 2) It is shown in Fig. 7 that the Relative Factor  $\alpha_2$  of the channel with the smaller singular value  $\beta_2$  can be significantly smaller than 1, which means the waterfilling scheme utilizing both two channels can have large fluctuations in channel capacity, shown in Fig. 8 and Fig. 9.
- 3) The distribution of the Relative Factor is similar when  $d_s$  is varied with fixed  $h_{ant}$  and  $d_{wall}$ , which is omitted here due to limited space.
- 4) For spatial variations in the antenna position on the order of 1 cm, the received signal power varies by less than 6.4 dB for all the three schemes, which is in stark contrast to the 46.7 dB variation observed in the SISO case. Furthermore, despite these small variations, the received power for both the dominant eigenmode scheme and the Alamouti code is always higher than the free space SISO benchmark.

**Channel Capacity:** We compute the channel capacity as we vary the wall distance or the antenna height with each of the three schemes. Under the same variations described for the received signal power, we wish to emphasize the following inferences from our simulations (see Fig. 8 and Fig. 9):

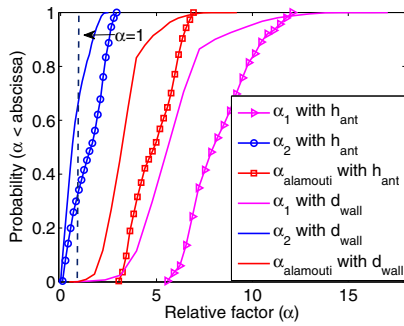


Fig. 7. CDF of the Relative Factor of  $2 \times 2$  MIMO channel

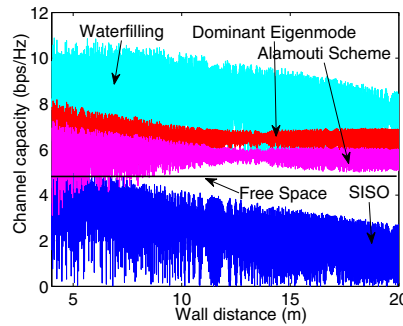


Fig. 8. Variation of channel capacity with the wall distances

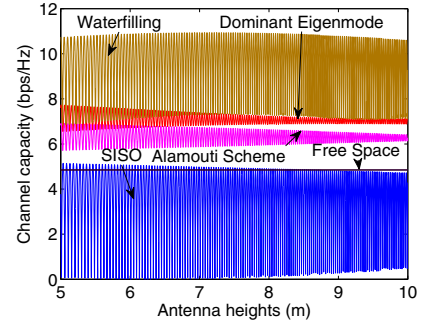


Fig. 9. Variation of channel capacity with the antenna heights

- 1) All the space-time schemes have significantly greater channel capacities than the capacity for the SISO free space propagation benchmark.
- 2) The SISO scheme is extremely fragile with variations in wall distance with channel capacities ranging from  $4.1 \times 10^{-4}$  bps/Hz to 5.4 bps/Hz (shown in Fig. 8).
- 3) As expected, the waterfilling scheme maximizes the channel capacity, but it also exhibits significant variation in channel capacity (4.3 - 10.9 bps/Hz) as the wall distance varies from 4 m to 20 m. On the other hand, the dominant eigenmode and the Alamouti schemes do not vary a lot with change in the wall distance. Once the wall distance is greater than 10m, these schemes vary at most by 1.3 bps/Hz.
- 4) The capacity exhibits quasi-periodic behavior as the reflected rays combine destructively/constructively when we vary the antenna height.

## V. CONCLUSION

We have shown that channel models for highly directional mm wave links are fundamentally different from those for the rich scattering environments corresponding to omnidirectional links at lower carrier frequencies. In the setting considered, a small number of strong paths account for fluctuations in the received signal strength. For a SISO link, the resulting fades are significant, and are extremely sensitive to small variations in geometric parameters such as antenna height, wall distance and range. However, we also show that a properly designed  $2 \times 2$  MIMO link can provide both the vertical and horizontal diversity required to combat such fading, with performance that improves upon an ideal SISO link with no fading.

While most issues related to signal processing and protocols for highly directional multiGigabit mm wave networks remain open, we mention some topics for future work which are specifically related to the issues discussed in this paper. The delay spread for the channels we have considered can be several times the symbol period for the multiGigabit links of interest. An important area for future work, therefore, is the design of strategies that account for the overall spatiotemporal channel. Another important area is the design of nodes for easy deployability and robust performance. For example, can we realize “omni-coverage” yet highly directional nodes providing electronic steerability over a  $360^\circ$  horizontal field

of view, while also providing the spatial diversity required for combating fading?

## REFERENCES

- [1] M. Luise, F. Giannetti, and R. Reggiannini, “Mobile and personal communications in the 60 GHz Band: a survey,” *Wireless Personal Communications*, vol. 10, no. 2, pp. 207-243, 1999.
- [2] C. H. Doan, S. Emarni, and et al., “Millimeter-wave CMOS design,” *IEEE J. Solid-State Circuits*, vol. 40, no. 1, Jan. 2005
- [3] S. K. Reynolds, B. A. Floyd, U. Pfeiffer, T. Beukema, J. Grzyb, and C. Haymes, “A Silicon 60-GHz Receiver and Transmitter Chipset for Broadband Communications,” *IEEE J. Solid-State Circuits*, vol. 41, no. 12, pp. 2820-2831, Dec. 2006.
- [4] P. Smulders, “Exploiting the 60 GHz band for local wireless multimedia access: Prospects and future directions,” *IEEE Commun. Mag.*, no. 1, pp. 140-147, Jan. 2002.
- [5] R. Mudumbai, S. Singh, and U. Madhow, “Medium access control for 60 GHz outdoor mesh networks with highly directional links,” in *Proc. IEEE INFORCOM 2009, Mini Conference*, Apr. 2009, pp. 2871-2875.
- [6] M.-S. Choi, G. Grosskopf, and D. Rohde, “Statistical Characteristics of 60 GHz wideband indoor propagation channel,” *Proc. IEEE PIMRC 2005*, vol. 1, pp. 599-603, Sept. 2005.
- [7] N. Moraitis and P. Constantinou, “Indoor channel measurements and characterization at 60 GHz for wireless local area network applications,” *IEEE Trans. Antennas Propag.*, vol. 52, no. 12, pp. 3180-3189, Dec. 2004.
- [8] H. Xu, V. Kukshya, and T. S. Rappaport, “Spatial and temporal characteristics of 60-GHz indoor channels,” *IEEE J. Select. Areas Commun.*, vol. 20, no. 3, pp. 620-630, Apr. 2002.
- [9] S. Geng, J. Kivinen, X. Zhao, and P. Vainikainen, “Millimeter-Wave Propagation Channel Characterization for Short-Range Wireless Communications,” *IEEE Vehicular Tech.*, vol. 58, no. 1, pp. 3-13, Jan. 2009.
- [10] N. Moraitis and P. Constantinou, “Indoor channel modeling at 60 GHz for wireless LAN applications,” *Proc. PIMRC 2002*, vol. 3, Lisbon, Portugal, Sept. 2002, pp. 1203-1207.
- [11] R. Mazar, A. Bronshtern, and I-Tai Lu, “Theoretical analysis of UHF propagation in a city street modeled as a random multislit waveguide,” *IEEE Trans. Antennas Propag.*, vol. 46, no. 6, pp. 864-871, Jun. 1998.
- [12] A. A. Abouda, N. G. Tarhuni, and H. M. El-Sallabi, “Effect of antenna array geometry and ULA azimuthal orientation on MIMO channel properties in urban city street grid,” *Progress in Electromagnetics Research*, PIER 64, pp. 257-278, 2006
- [13] P. F. M. Smulders, “Deterministic modelling of indoor radio propagation at 40-60 GHz,” *Wireless Pers. Commun.*, vol. 1, no. 2, Jun. 1994
- [14] M. Seo, B. Ananthasubramaniam, M. Rodwell, and U. Madhow, “Millimeterwave imaging sensor nets: a scalable 60-GHz wireless sensor network,” *2007 IEEE MTT-S Int. Microwave Symp. Dig.*, June 2007.
- [15] E. Biglieri, R. Calderbank, A. Constantinides, A. Goldsmith, A. Paulraj, and H. V. Poor. “MIMO Wireless Communications.” Cambridge University Press, 2007.
- [16] A. Goldsmith, *Wireless communications*. Cambridge Univ. Press, 2005
- [17] S. Alamouti, “A simple transmit diversity technique for wireless communications,” *IEEE J. Sel. Areas Comm.*, vol.16, no. 8, pp. 1451-1458, Oct. 1998.
- [18] B. Langen, G. Lober, and W. Herzig, “Reflection and transmission behavior of building materials at 60 GHz,” in *Proc. IEEE PIMRC '94*, Hague, Netherlands, pp. 505-509. Sept. 1994.